

Structure and luminescence of α-plane GaN on γ-plane sapphire substrate modified by Si implantation

Lijie Huang(黄黎杰), Lin Li(李琳), Zhen Shang(尚震), Mao Wang(王茂), Junjie Kang(康俊杰), Wei Luo(罗巍), Zhiwen Liang(梁智文), Slawomir Prucnal, Ulrich Kentsch, Yanda Ji(吉彦达), Fabi Zhang(张法碧), Qi Wang(王琦), Ye Yuan(袁冶), Qian Sun(孙钱), Shengqiang Zhou(周生强), Xinqiang Wang(王新强)

Citation: Chin. Phys. B, 2021, 30 (**5**): 056104. DOI: 10.1088/1674-1056/abd76a
Journal homepage: http://cpb.iphy.ac.cn; http://iopscience.iop.org/cpb

What follows is a list of articles you may be interested in

Evolution of ion-irradiated point defect concentration by cluster dynamics simulation

Shuaishuai Feng(冯帅帅), Shasha Lv(吕沙沙), Liang Chen(陈良), Zhengcao Li(李正操)
Chin. Phys. B, 2021, 30 (**5**): 056105. DOI: 10.1088/1674-1056/abf102

Defects and electrical properties in Al-implanted 4H-SiC after activation annealing

Yi-Dan Tang(汤益丹), Xin-Yu Liu(刘新宇), Zheng-Dong Zhou(周正东), Yun Bai(白云), Cheng-Zhan Li(李诚瞻)
Chin. Phys. B, 2019, 28 (**10**): 106101. DOI: 10.1088/1674-1056/ab3cc2

Structural and electrical properties of carbon-ion-implanted ultrananocrystalline diamond films

Hui Xu(徐辉), Jian-Jun Liu(刘建军), Hai-Tao Ye(叶海涛), D J Coathup, A V Khomich, Xiao-Jun Hu(胡晓君)
Chin. Phys. B, 2018, 27 (**9**): 096104. DOI: 10.1088/1674-1056/27/9/096104

Wettability of Si and Al-12Si alloy on Pd-implanted 6H-SiC

Ting-Ting Wang(汪婷婷), Gui-Wu Liu(刘桂武), Zhi-Kun Huang(黄志坤), Xiang-Zhao Zhang(张相召), Zi-Wei Xu(徐紫巍), Guan-Jun Qiao(乔冠军)
Chin. Phys. B, 2018, 27 (**4**): 046101. DOI: 10.1088/1674-1056/27/4/046101

Structural and size evolution of indium nanoparticles embedded in aluminum synthesized by ion implantation

Yan-Xia Yan(晏艳霞), Meng Liu(刘孟), Mei-Juan Hu(胡梅娟), Hong-Zhi Zhu(朱宏志), Huan Wang(王欢)
Chin. Phys. B, 2017, 26 (**12**): 126101. DOI: 10.1088/1674-1056/26/12/126101

SPECIAL TOPIC — Ion beam modification of materials and applications

Structure and luminescence of a-plane GaN on r-plane sapphire substrate modified by Si implantation*

Lijie Huang(黄黎杰)[1,7], Lin Li(李琳)[2,3], Zhen Shang(尚震)[2], Mao Wang(王茂)[2], Junjie Kang(康俊杰)[1], Wei Luo(罗巍)[1], Zhiwen Liang(梁智文)[5], Slawomir Prucnal[2], Ulrich Kentsch[2], Yanda Ji(吉彦达)[4], Fabi Zhang(张法碧)[7], Qi Wang(王琦)[5], Ye Yuan(袁冶)[1,†], Qian Sun(孙钱)[6], Shengqiang Zhou(周生强)[2], and Xinqiang Wang(王新强)[1,5]

[1] *Songshan Lake Materials Laboratory, Dongguan* 523808, *China*
[2] *Helmholtz-Zentrum Dresden-Rossendorf, Institute of Ion Beam Physics and Materials Research,* 01314, *Dresden, Germany*
[3] *College of Mathematics and Physics, Beijing University of Chemical Technology, Beijing* 100029, *China*
[4] *Department of Applied Physics, College of Science, Nanjing University of Aeronautics and Astronautics, Nanjing* 211106, *China*
[5] *Dongguan Institute of Optoelectronics, Peking University, Dongguan* 523808, *China*
[6] *Key Laboratory of Nanodevices and Applications, Suzhou Institute of Nano-Tech and Nano-Bionics (SINANO), Chinese Academy of Sciences (CAS), Suzhou* 215123, *China*
[7] *Guangxi Key Laboratory of Precision Navigation Technology and Application, Guilin University of Electronic Technology, Guilin* 541004, *China*

(Received 10 November 2020; revised manuscript received 27 December 2020; accepted manuscript online 30 December 2020)

We show the structural and optical properties of non-polar a-plane GaN epitaxial films modified by Si ion implantation. Upon gradually raising Si fluences from 5×10^{13} cm^{-2} to 5×10^{15} cm^{-2}, the n-type dopant concentration gradually increases from 4.6×10^{18} cm^{-2} to 4.5×10^{20} cm^{-2}, while the generated vacancy density accordingly raises from 3.7×10^{13} cm^{-2} to 3.8×10^{15} cm^{-2}. Moreover, despite that the implantation enhances structural disorder, the epitaxial structure of the implanted region is still well preserved which is confirmed by Rutherford backscattering channeling spectrometry measurements. The monotonical uniaxial lattice expansion along the a direction (out-of-plane direction) is observed as a function of fluences till 1×10^{15} cm^{-2}, which ceases at the overdose of 5×10^{15} cm^{-2} due to the partial amorphization in the surface region. Upon raising irradiation dose, a yellow emission in the as-grown sample is gradually quenched, probably due to the irradiation-induced generation of non-radiative recombination centers.

Keywords: ion implantation, GaN, defects

PACS: 61.72.uj **DOI:** 10.1088/1674-1056/abd76a

1. Introduction

The strong c-axis polarization in wurtzite nitride semiconductor has been regarded as one of main obstacles to prohibit overall application in optoelectronic device. For example, the polarization-induced quantum confine Stark effect prevents the recombination between holes and electrons in the charge area.[1–3] The enhanced polarization also causes the irradiation transformation from transverse-electric to transverse-magnetic model, therefore decreases the illumination area in light-emitting diode (LED).[4–6] Therefore, to solve the dilemma induced by such a polarization along the c axis in nitride semiconductor, a lot of efforts have been devoted to the development of non-polar face nitride compounds.[7–9] However, the doping in non-polar face GaN growth is relatively hard when compared with in conventional c-face GaN due to the different growth processes. Ion implantation acts as a proper solution to fulfill the requirement by implanting Si or Mg ions into GaN matrix, afterwards annealing treatment is employed to activate implanted dopants. Therefore, it is meaningful to track the ion implantation-induced modification,[10] *e.g.*, crystalline damages and strain, in the as-implanted matrix in order to predetermine the optimal annealing parameters. Actually, several efforts have been made on Si- or Mg-implanted c-plane GaN,[11–13] however the study on the non-polar a- or m-plane GaN is still limited.

In the present work, the structural modification of Si-implanted GaN is systematically investigated by various methods. According to the analysis by Rutherford backscattering/channeling spectrometry (RBS/C) and polarized Raman, the epitaxial nature of the implanted layer is well preserved with the presence of lattice disorder. Additionally, the implanted layer presents a uniaxial lattice expansion along the out-of-plane direction. Regarding the luminescence behavior, both the near bandgap emission and the yellow band emission are gradually quenched with increasing implantation fluence, probably due to the irradiation-induced non-radiative recom-

*Project supported by the Key-Area Research and Development Program of Guangdong Province, China (Grant Nos. 2019B010132001, 2020B010174003, and 2019B121204004), the Basic and Application Basic Research Foundation of Guangdong Province, China (Grant Nos. 2020A1515110891 and 2019A1515111053), and the Fund from the Ion Beam Center (IBC) at HZDR.

†Corresponding author. E-mail: yuanye@sslab.org.cn

© 2021 Chinese Physical Society and IOP Publishing Ltd

bination centers.

2. Experiment

The non-polar *a*-plane GaN samples were grown on *r*-sapphire by horizontal metalorganic chemical vapor deposition (MOCVD). Before the GaN preparation, a 60-nm thick AlN was pre-grown at 1150 °C as a buffer. Subsequently, a three-dimensional (3D) growth mode of GaN was introduced at a pressure of 200 mbar (1 bar = 10^5 Pa) and with a V/III ratio of 2162 to control the growth dynamics, and the thickness of GaN is around 2 μm. More details about the as-grown sample were discussed in Refs. [14,15]. To achieve more uniform distribution of Si in GaN, a bi-implantation with energies of 100 eV and 30 keV was set, and the wafer normal was tilted by 7° with respect to the ion beam to avoid channeling. Four samples were implanted. The implantation fluences at 100 keV were 4×10^{13}, 2×10^{14}, 8×10^{14}, and 4×10^{15}. The corresponding fluences at 30 keV were 1×10^{13}, 5×10^{13}, 2×10^{14}, and 1×10^{15} cm^{-2}, respectively. Sample names are entitled as GaN 1, GaN 2, GaN 3, and GaN 4, accordingly. To make a comparison, an as grown sample named as GaN virgin is picked up as a reference. The lattice damage of the Si implanted *a*-plane GaN was investigated by Rutherford backscattering spectrometry (RBS)/channeling spectrometry. During the RBS measurement, a collimated 1.7-MeV He^+ beam with a 10 nA–20 nA beam current of 10 nA–20 nA was applied, and the scattered ions were collected at a backscattering angle of 170°. The channeling spectra were recorded by aligning the GaN $[2\bar{1}\bar{1}0]$ axis parallel to the impinging He^+ beam. Raman measurements were performed in the backscattering geometry using the 532-nm line of a Nd:YAG laser by treating the out-of-plane direction as *x* axis, in $x(zz)\bar{x}$ and $x(yy)\bar{x}$ backscattering configurations using a LabRam HR800 spectrometer (HORIBA Jobin Yvon GmbH, Bensheim, Germany) aided with an optical microscope Olympus BX40 (Olympus Corporation, Hamburg, Germany). A 40× objective lens was used to focus the laser beam and to collect the Raman signal. X-ray diffraction (XRD) measurements were performed on a Panalytical Empyrean diffractometer equipped with an Anton-paar DHS 1100 domed hot stage. The Cu target emitted x-ray was filtered with a 1/4 slit and then further filtered with a commercial Ge (220) hybrid monochromator for a highly collimated K_{a1} beam (1.54059-Å wavelength). The radius of the diffraction circle is 240 mm. The PIXcel one-dimensional (1D) detector has 256 matrix channels, and the resolution for each channel is 55 lm. The optical properties of the as-grown and irradiated GaN thin films were investigated by room-temperature photoluminines (PL), and the measurements were excited by a 405-nm laser coupled to a monochromator for the selective PL excitation. The emitted PL light from the sample was guided through a set of lenses and a long pass filter to a Jobin Yvon Triax 320 monochromator and then recorded by a Hamamatsu Si photomultiplier.

3. Results and discussion

According to the simulation by the stopping and range of ions in matter (SRIM) code,[16] the depth dependent distribution of implanted Si atoms and generated vacancies are shown in Fig. 1. In Fig. 1(a), it is clearly observed that the distribution of Si atoms presents bi-maximal signals at the depth of 25 nm and 100 nm, respectively, which is ascribed to the process of bi-implantation. Fortunately, in the near surface 100-nm depth, the concentration of Si dopant presents quasi-constant and the average value is 4.6×10^{18}, 2.3×10^{19}, 9.1×10^{19}, and 4.5×10^{20} cm^{-3} for samples GaN 1, GaN 2, GaN 3, and GaN 4, respectively. Actually, during the implantation process, due to collisions between implanted ions and atoms in the lattice, various types of vacancies are produced in the matrix where the implantation fluence is not sufficient high to totally amorphize the target region. Accordingly, the densities of generated vacancies are calculated by SRIM. In agreement with the implanted dopant distribution, the produced vacancies distribute constantly in the surficial 100-nm region, and the depth profiles are shown in Fig. 1(b). Upon gradually increasing the implantation fluence, the vacancy densities are calculated as 3.7×10^{21}, 1.8×10^{22}, 7.1×10^{22}, and 3.7×10^{23} cm^{-3}, respectively. However, the immediate vacancy recombination during the irradiation process is no considered in the SRIM calculation, therefore the real vacancy densities are far below the simulated values. The structural and optical properties will be displayed and discussed in the next sections.

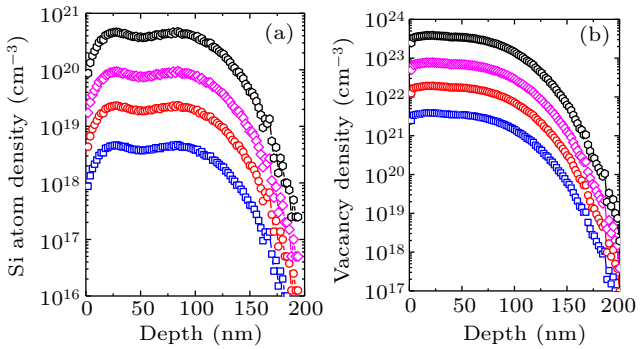


Fig. 1. Stopping and range of ions in matter (SRIM) calculated (a) silicon ion distribution (squares) and (b) induced vacancy distribution profiles for samples GaN 1 (squares), GaN 2 (circles), GaN 3 (diamonds), and GaN 4 (hexagons). The calculation does not consider the dynamic recombination. Most of the vacancies recombine immediately after the collision. The real vacancy density is much smaller than the calculated one.

Figure 2 shows RBS random and channeling spectra of all implanted GaN samples. The ion-channeling behavior, the large reduction of the backscattering yield when the He-beam is along the crystalline axis, is very prominent even though the Si implantation fluence is as high as 5×10^{15} cm^{-2}. This verifies their preservation of epitaxially single-crystalized nature and no signature of large-scale amorphization is observed.[17,18] The minimum yield (χ_{min}), which

is defined as the yield-ratio between the channeling and random signal, can be used for assessing the quality of crystallization. Herein, the χ_{min} (energy from 1200 keV to 1250 keV) are calculated as 1.8%, 3.5%, 5.8%, and 8.0% for samples GaN 1, GaN 2, GaN 3, and GaN 4, respectively. The low value of 1.8% implies the fact that the quality of the sample GaN 1 is comparable with the *c*-GaN single-crystal.[19–21] However, upon increasing implantation fluences, the gradually raised χ_{min} indicates the lattice disorder. Particularly, the increasing backscattering yield at 706 and 753 channel numbers in the inset of Fig. 2 suggests that the implantation-caused defects gradually accumulate at the near surface and the projected range. Such an effect has been observed in implanted *c*-plane GaN.[13,19,22] Actually, such a surficial disorder results from the fact that during implantation process there is decomposition of GaN and N is preferentially sputtered. Therefore, after ion implantation the surface is damaged and Ga-rich. This phenomenon indicates that it is necessary to add a capping layer to prevent the N evaporation before the implantation.

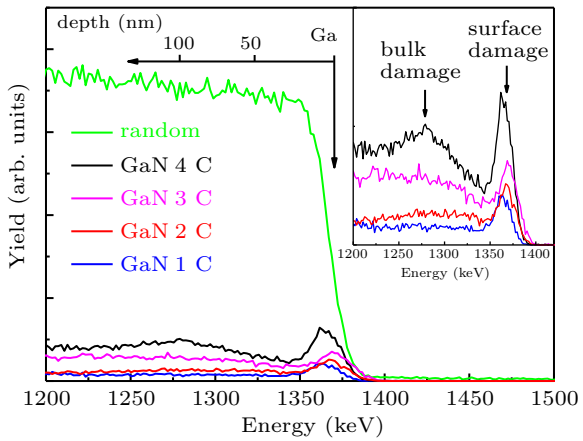


Fig. 2. RBS random and $\langle 2\bar{1}\bar{1}0\rangle$ aligned channeling spectra (C) of samples of GaN 1, GaN 2, GaN 3, and GaN 4, respectively. The random spectra of all samples are the same since the signal of Si is too weak and only one of them is present. Inset: Zoom of channeling spectra from energy 1200 keV to 1450 keV.

In order to further explore the structural information of Si-implanted *a*-plane GaN, the Raman spectroscopy is used at two geometries of $x(z,z)\bar{x}$ and $x(y,y)\bar{x}$ by defining the out-of-plane direction as the x axis, and aligning y and z axes in the basal face and along the c axis of the GaN hexagon structure, respectively. As shown in Fig. 3, the first order phonon scattering peaks from GaN and Al_2O_3 are observed, however the signal from AlN buffer is invisible. As previous study, the peaks at wave numbers of 378, 416, 429, 448, and 643 cm^{-1}, correspond to E_g, A_{1g}, E_g, E_g, and A_{1g} modes from Al_2O_3 substrate.[23,24] Interestingly, although the wavenumber of one GaN second-order Raman signal (418 cm^{-1}) is consistent with the peak at 416 cm^{-1}, its strong intensity excludes such an assumption. In the case of GaN, four first-order vibration modes, $A_1+E_1+2E_2$, are Raman-active at the Γ point, although there are eight sets of predicted phonon modes in the C_{6v}^4 space group: $2A_1+2E_1+2B_1+2E_2$ of which one A_1 and E_1 modes are acoustic and two B_1 modes are silent.[25] Of above-mentioned four Raman-sensitive modes, A_1 and E_1 symmetries are polar thus can split into transverse (TO) and longitudinal (LO) components.[26] In the backscattering configurations of $x(z,z)\bar{x}$ and$x(y,y)\bar{x}$, the selection rules only predict the presence of A_1(TO) and A_1(TO) + E_2(TO), respectively,[25] which seems to be violated by our results shown in Fig. 3. It is worth noting that the observation of small E_1(TO) signal in both cases has been discussed in previous works:[27] The incident and scattered lights are not precisely parallel with the coordinate axis due to the introduced defects during the growth of non-polar GaN. Those defects result in the so-called disorder-activated Raman scattering (DARS) mode.

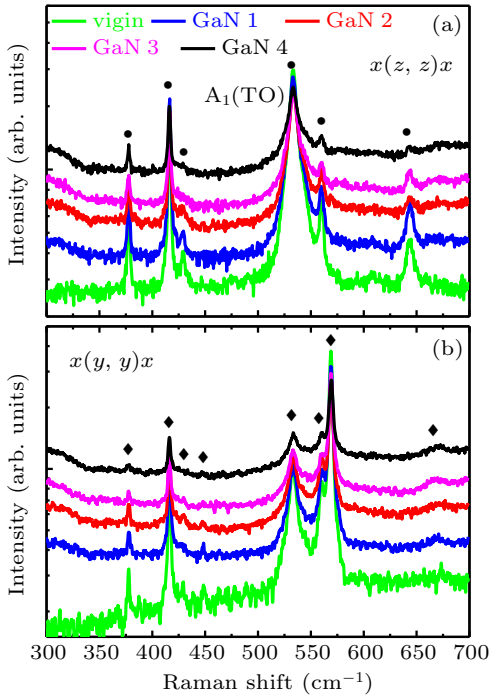


Fig. 3. Polarized Raman scattering spectra of *a*-plane GaN at the surface geometry of (a) $x(z,z)\bar{x}$ and (b) $x(y,y)\bar{x}$. The x axis is along the GaN a axis (out-of-plane direction), while y and z axes are along the m and c axes (both are in the plane), respectively.

If only A_1, E_1, and E_2 resonance peaks from GaN are considered, with gradually increasing implantation fluences, all Raman peaks keep their original frequencies, however their intensity declines and the linewidth raises. By multi-peak fitting, the linewidth of three peaks is obtained, and the values are shown in Figs. 6(b) and 6(c). Actually, the linewidth is used to evaluate the perfection of the crystal. In addition to the A_1(TO) signal at the $x(yy)\bar{x}$ geometry, the linewidth of all peaks enhances, again indicating that the implantation is destructive to the crystal lattice. At the measurement minimal edge at 300 cm^{-1}, an upturn instead of a sharp peak is seen for all implanted samples but absent in the as-grown sample. This has been observed in various ion irradiated *c*-plane GaN according to previous study,[28] and it is ascribed to the highest acoustic-phonon branch at the zone boundary.[28,29]

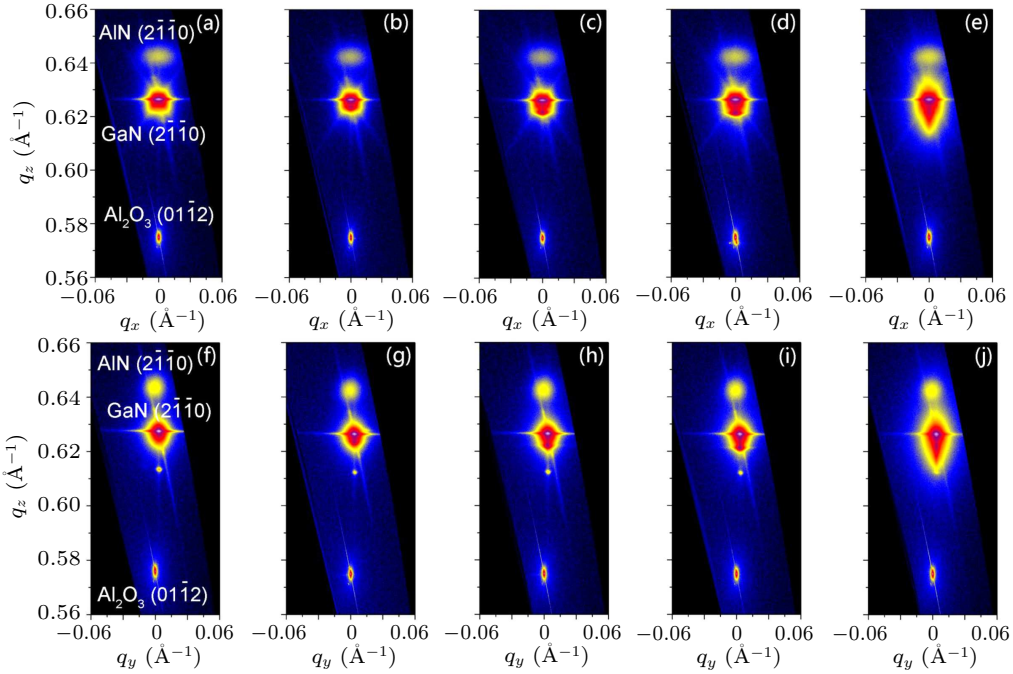


Fig. 4. The high-resolution reciprocal space mappings (RSM) of [(a)–(e)] q_z–q_x and [(f)–(j)] q_z–q_y modes for samples [(a), (f)] virgin *a*-plane GaN, [(b), (g)] GaN 1, [(c), (h)] GaN 2, [(d), (i)] GaN 3, and [(e), (j)] GaN 4 at around GaN (2$\bar{1}\bar{1}$0) peak.

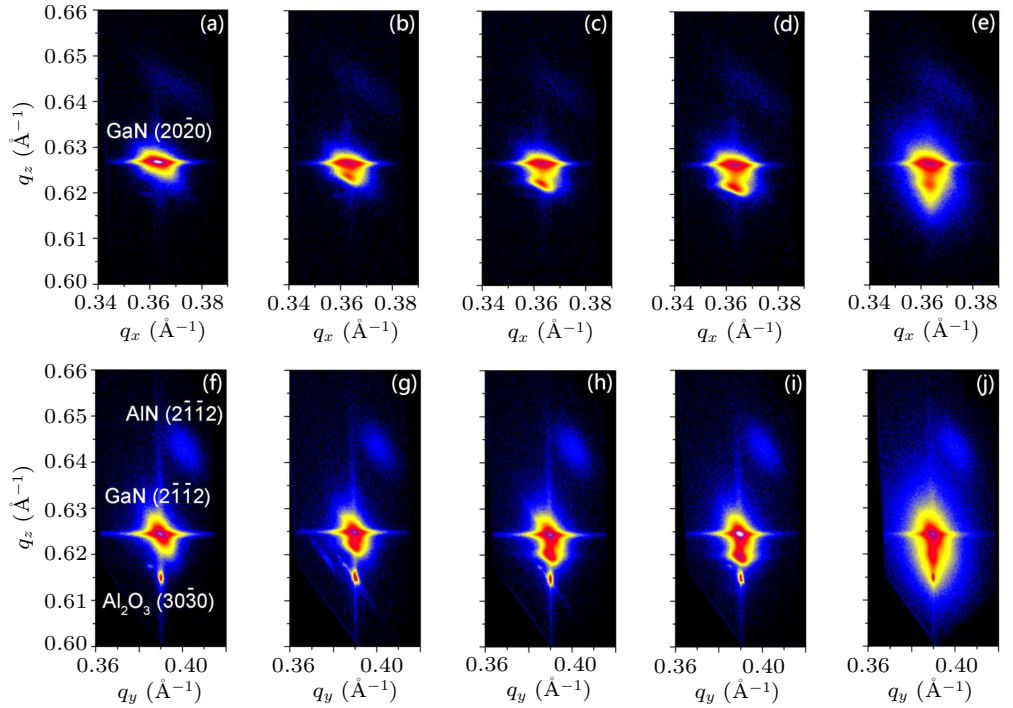


Fig. 5. The high-resolution RSM of [(a), (f)] virgin *a*-plane GaN, [(b), (g)] GaN 1, [(c), (h)] GaN 2, [(d), (i)] GaN 3, and [(e), (j)] GaN 4 at around (20$\bar{2}$0) [(a)–(e)] and (2$\bar{1}\bar{1}$2) peaks [(f)–(j)] of GaN.

According to previous studies, ion irradiation results in the expansion of lattice in both *a*-plane and *c*-plane GaN.[30,31] Therefore, systematic investigations are performed based on high-resolution XRD reciprocal space mapping of around (2$\bar{1}\bar{1}$0), (20$\bar{2}$0), and (2$\bar{1}\bar{1}$2) peaks, and the results are shown in Figs. 4 and 5. In all RSM results, the implanted samples give rise to two peaks. One is located as the same coordinate as in the virgin sample, and the second reveals lattice expansion. This implies that the whole GaN layer can be described as a combination of an irradiated region and another unirradiated region along the depth. The latter corresponds to the virgin film. In the as-grown sample, the out-of-plane lattice spacing along (2$\bar{1}\bar{1}$0) corresponding to the *a* axis is 1.5963 Å. On the basis of measured (20$\bar{2}$0) and (2$\bar{1}\bar{1}$2) peaks, the derived in-plane lattice constant of (0002) and (02$\bar{2}$0) planes are about 2.5858 Å and 1.3771 Å, respectively. When compared with the values of bulk GaN: 1.5950, 2.5945, and 1.3813 Å for (2$\bar{1}\bar{1}$0), (0002), and (02$\bar{2}$0) planes, respectively, our as-grown

a-plane GaN on *r*-plane sapphire undergoes tensile strain from the substrate. Upon increasing fluences, the measured three planes all exhibit expansion behavior given by the decreased q_z value till the sample GaN 3. As shown in Figs. 6(d) and 6(g), the lattice parameter saturates when the irradiation fluence reaches 5×10^{15} cm^{-2}, and this is probably interpreted by the surface amorphization resulted from high irradiation dose.

By playing the diffraction vector in the reciprocal space, the evolution of lattice parameters of planes $(02\bar{2}0)$ (along the *m* axis) and (0002) (along the *c* axis) are tracked, as displayed in Figs. 6(e) and 6(f). Interestingly, neither monotonical change nor obvious lattice distortion is seen for above-mentioned two planes, which is similar to Eu-implanted *a*-plane GaN.[30] In our case, although $(20\bar{2}0)$ planes are somehow equal to $(02\bar{2}0)$ planes in the bulk materials, the $(20\bar{2}0)$ plane exhibits expansion due to the fact that it is equipped with an out-of-plane component vector. Therefore, it is concluded that raising irradiation fluence results in the uniaxial expansion of lattice along the out-of-plane direction till the presence of high-dense defects induced by over-dosed implantation. In addition to GaN diffraction signals, several peaks nearby from the AlN buffer and Al_2O_3 are also detected, as shown in Figs. 4 and 5, however, since the implanted layer is far away from them, thus none of any peak-shifting is observed.

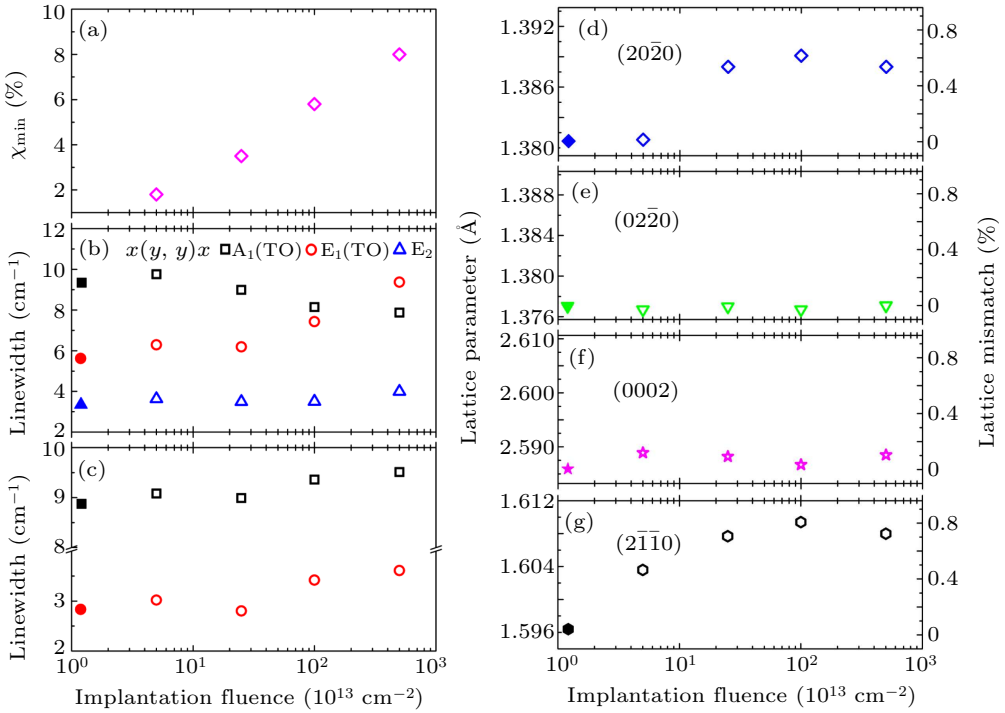


Fig. 6. The implantation fluence dependence of (a) χ_{min}, (b) and (c) Raman linewidth as well as lattice parameters (left) and lattice mismatch (right) of (d) $(20\bar{2}0)$, (e)$(02\bar{2}0)$, (f) (0002), and (g) $(2\bar{1}\bar{1}0)$ diffraction peaks.

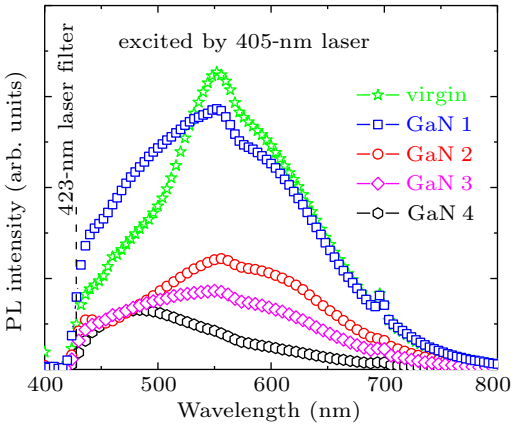


Fig. 7. Photoluminescence spectra of samples excited by 405-nm laser.

To examine the optical properties of the ion implanted *a*-plane GaN, photoluminescence was measured by 325-nm and 405-nm excitations. Interestingly, for 325-nm excited measurements, all implanted samples present quenched PL emission even including the near band edge. The results measured by 405-nm excitation are displayed in Fig. 7, and a strong yellow luminescence is observed in the as-grown sample. According to previous studies, the origin of such zero-phonon energy yellow luminescence has been under debate for a long time in the past decades: the emission may result from the transition between deep level impurity states and undefined energy level, *e.g.*, shallow donor[32–34] or conduction band edge.[35] Actually, it has been reported that the *a*-plane GaN grown on *r*-face sapphire by hydride vapor phase epitaxy as well as some other types of as-grown GaN exhibit similar strong yellow light emission.[36] In our case, upon increasing irradiation fluences, such a yellow emission is gradually suppressed, as shown in Fig. 7. Actually, a similar quench phenomenon, particularly for the yellow emission, has been

observed in electron irradiated GaN.[37] It is most likely due to that induced defects create a lot of non-radiative recombination centers.

4. Conclusion

By fully employing RBS, polarized Raman and high-resolution reciprocal space mapping by XRD, systematic investigations are performed for Si-implanted non-polar *a*-plane GaN epitaxial layers. With increasing implantation fluence, disorder is introduced into the matrix although the sample still keeps the epitaxial nature. The implantation-induced defects result in the uniaxial lattice expansion along the out-of-plane direction and the broadening of the Raman peaks. Moreover, the intensity of both the near band and yellow band emission is largely quenched with increasing the implantation fluence. It is probably due to the fact that the implantation generates the new competing recombination centers, particularly non-radiative ones. These results provide useful information for using ion implantation as a doping approach for non-polar GaN.

References

[1] Kane M H and Arefin N 2014 *Nitride Semiconductor Light-Emitting Diodes (LEDs)* pp. 99–143
[2] Miller D A B, Chemla D S, Damen T C, Gossard A C, Wiegmann W, Wood T H and Burrus C A 1984 *Phys. Rev. Lett.* **53** 2173
[3] Takeuchi T, Sota S, Katsuragawa M, Komori M, Takeuchi H, Amano H and Akasaki I 1997 *Jpn. J. Appl. Phys.* **36** L382
[4] Reich C, M. Guttmann, M. Feneberg, Wernicke T, Mehnke F, Kuhn C, Rass J, Lapeyrade M, Einfeldt S, Knauer A, Kueller V, Weyers M, Goldhahn R and Kneissl M 2015 *Appl. Phys. Lett.* **107** 142101
[5] Li X H, Kao T T, Satter M M, Wei Y O, Wang S, Xie H, Shen S C, Yoder P D, Fischer A M, Ponce F A, Detchprohm T, Dupuis R D 2015 *Appl. Phys. Lett.* **106** 041115
[6] Nagasawa Y and Hirano A 2018 *Appl. Sci.* **8** 1264
[7] Iso K, Yamada H, Hirasawa H, Fellows N, Saito M, Fujito K, DenBaars S P, Speck J S and Nakamura S 2007 *Jpn. J. Appl. Phys.* **46** L960
[8] Holder C, Speck J S, DenBaars S P, Nakamura S and Feezell D 2012 *Appl. Phys. Express* **5** 092104
[9] Kim K C, Schmidt M C, Sato H, Wu F, Fellows N, Saito M, Fujito K, Speck J S, Nakamura S and DenBaars S P 2007 *Phys. Status Solidi Rapid Res. Lett.* **1** 125
[10] Lorenz K, Wendler E, Cubero A R, Catarino N, Chauvat M P, Schwaiger S, Scholz F, Alves E and Ruterana P 2017 *Acta Materialia* **123** 177
[11] Zolper J C, Tan H H, Williams J S, Zou J, Cockayne D J H, Pearton S J, Crawford M H and Karlicek Jr R F 1997 *Appl. Phys. Lett.* **70** 2729
[12] Pong B J, Pan C J, Teng Y C, Chi G C, Li W H and Lee K C 1998 *J. Appl. Phys.* **83** 5992
[13] Kobayashi H and Gibson W M 1998 *Appl. Phys. Lett.* **73** 1406
[14] Sun Q, Ko T S, Yerino C D, Zhang Y, Lee I H, Han J, Lu T C, Kuo H C and Wang S C 2009 *Jpn. J. Appl. Phys.* **48** 071002
[15] Kong B H, Sun Q, Yerino C D, Ko T S, Leung B, Cho H K and Ha J 2009 *J. Appl. Phys.* **106** 123519
[16] Ziegler J F 2004 *Nucl. Instrum. Methods Phys. Res. B* **219** 1027
[17] Lorenz K, Wahl U, Alves E, Wojtowicz T, Ruteran P, Ruffenach S and Briot O 2004 *Superlattices Microstruct.* **36** 737
[18] Azarov A Y, Jensen J, Hallén A and Aggerstam T 2008 *J. Appl. Phys.* **104** 053509
[19] Usman M, Hallén A, Nazir A 2015 *J. Phys. D: Appl. Phys.* **48** 455107
[20] Parikh N, Suvkhanov A, Lioubtchenko M, Carlson E, Bremser M, Bray D, Davis R and Hunn J 1997 *Nucl. Instrum. Methods Phys. Res. B* **127128** 463
[21] Kobayashi H and Gibson W M 1999 *J. Vac. Sci. Technol.* **17** 2132
[22] Lorenz K, Wahl U, Alves E, Dalmasso S, Martin R W, O'Donnell K P, Ruffenach S, Briot O 2004 *Appl. Phys. Lett.* **85** 2712
[23] Kadleikova M, Breza J and Vesely M 2001 *Microelectronics J.* **32** 955
[24] Porto S P S and Krishnan R S 1967 *J. Chem. Phys.* **47** 1009
[25] Harima H 2002 *J. Phys.: Condens. Matter.* **14** R967
[26] Murugkar S and Merlin R 1995 *J. Appl. Phys.* **77** 6042
[27] Gao H, Yan F, Zhang H, Li J, Wang J and Yan J 2007 *J. Appl. Phys.* **101** 103533
[28] Limmer W, Ritter W, Sauer R, Mensching B, Liu C and Rauschenbach B 1998 *Appl. Phys. Lett.* **72** 2589
[29] Siegle H, Kaczmarczyk G, Filippidis L, Litvinchuk A P, Hoffmann A and Thomsen C 1997 *Phys. Rev. B* **55** 7000
[30] Catarino N, Nogales E, Franco N, Darakchieva V, Miranda S M C, Mendez B, Alves E, Marques J G and Lorenz K 2012 *Europhys. Lett.* **97** 68004
[31] Liu C, Mensching B, Volz K and Rauschenbach B 1997 *Appl. Phys. Lett.* **71** 2313
[32] Julkarnain N K M, Fukuda T and Arakawa Y 2016 *Opt. Mater.* **60** 481
[33] Reshchikov M A, McNamara J D, Zhang F, Monavarian M, Usikov A, Helava H, Makarov Y and Morkoç H 2016 *Phys. Rev. B* **94** 035201
[34] Hofmann D M, Kovalev D, Steude G, Meyer B K, Hoffmann A, Eckey L, Heitz R, Detchprom T, Amano H and Akasaki I 1995 *Phy. Rev. B* **52** 16702
[35] Chen H M, Chen Y F, Lee M C and Feng M S 1997 *Phys. Rev. B* **56** 6942
[36] Lee M, Vu T K O, Lee K S, Kim E K and Park S 2018 *Sci. Rep.* **8** 7814
[37] Buyanova I A, Wagner M, Chen W M, Monemar B, Lindström J L, Amano H and Akasaki I 1998 *Appl. Phys. Lett.* **73** 2968